Progress In Electromagnetics Research, Vol. 129, 579–601, 2012

PERFORMANCE ANALYSIS OF POLARIZATION-SPACE-TIME THREE-DOMAIN JOINT PROCESSING FOR CLUTTER SUPPRESSION IN AIRBORNE RADAR

D. Wu*, Z. Xu, L. Zhang, Z. Xiong, and S. Xiao

School of Electronic Science and Engineering, National University of Defense Technology, Changsha 410073, China

Abstract—An optimum polarization-space-time joint domain processing (PST-JDP) technique is proposed for clutter suppression which adequately adopts the three-domain information including the polarization, space and Doppler frequency information of the radar echo. The study shows that the polarization information together with the space and Doppler frequency information are effective to significantly enhance the clutter suppression performance for airborne radar. Several new techniques, (i.e., the covariance matrix eigendecomposition, the spectral analysis and the resolution grid method), are utilized for deriving the performance of the optimum PST-JDP. The main factors which affect on the performance of clutter rejection are the clutter degree of polarization, statistical distance of polarization between target and clutter, Doppler frequency of target and input clutter-to-noise ratio. The new optimum PST-JDP method outperforms significantly the traditional optimum space-time processing technology, especially in the case of the slowly or tangentially moving target. The simulation verifies the correctness and efficiency of the model.

1. INTRODUCTION

Clutter suppression or the detection of weak targets in heavy clutter environments is considered a challenging problem, mainly because it is not possible to discriminate the target from the clutter in the Doppler frequency domain. Many techniques were proposed and analyzed to suppress clutter in one or twodomain [1–4], which enhanced the out of signal-to-clutter-plus-noise ratio (SCNR) and improved the target detectability, discrimination and resolution. Figure 1 summarizes the methods for clutter suppression in different domains.

Received 21 May 2012, Accepted 2 July 2012, Scheduled 16 July 2012

* Corresponding author: Dijun Wu (dijunwu@sina.com).

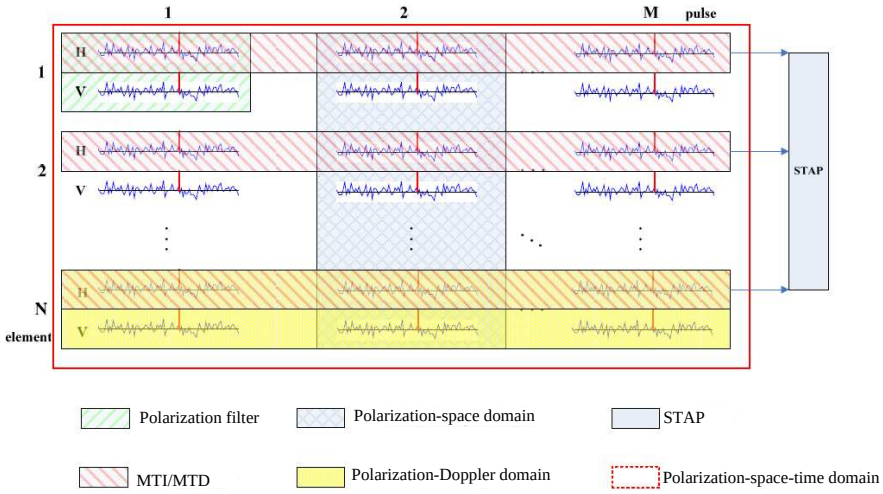

Figure 1. The method of clutter suppression in different domains.

The methods in one domain contain adaptive polarization filter and moving target detection (MTI). The early developments of polarization techniques may be traced back to 1950s [5]. There are many polarimetric filtering techniques which contain adaptive polarization cancellation (APC) [6] virtual polarization adaptation (VPA) technique [7, 8], multi-notch logic-product (MLP) polarization filter [9] and adaptive polarimetric filter [10–14]. However, all of techniques have a common problem that both the target and clutter/interference may be cancelled when they have a similar polarization. This problem can be partially solved by altering radar transmit polarization parameters to vary the polarization response of the target and clutter [15–19], which maybe enlarge the polarization difference between the target and clutter in polarization domain. MTI filter suppresses clutter at integer multiples of the pulse repetition frequency (PRF) in time domain, and allows to return from moving targets to pass through with little or no degradation [20]. The common methods are two pulses canceller and three pulses canceller. However, the performance of MTI becomes serious when the target Doppler frequency is small.

The techniques of clutter suppression in two joint domains contain space time adaptive processing (STAP), polarization-Doppler joint processing and polarization-space joint domain processing Polarization-space joint domain processing [21–25] is mainly utilized to reject jamming from different direction. Polarization-Doppler

joint processing for coherent radar were studied in Gaussian and non-Gaussian background [26, 27], which has used fully polarization and Doppler information of target to suppress clutter and enhance detection probability. The researches results have been demonstrated by IPIX radar measure data. However, it is difficult to discriminate the target and clutter when they are similar to each other in the polarization domain and Doppler domain. The effort on the development of space-time adaptive processing technique of clutter suppression may be traced back to the 1970s [28] with the clutter covariance matrix (CCM) assumed to be known. The sample matrix inversion (SMI) algorithm has been developed [29] to replace with the covariance matrix estimate. In the middle of 1980s, Kelly presented the generalized likelihood ratio (GLR) test algorithm in the case of unknown covariance matrix and the target amplitude [30]. In the complex electromagnetic environment, the clutter environment is always nonhomogeneous and nonstationary, which leads to a straightforward application of the data domain SMI or GLR algorithm performance degradation. Therefore, aiming at the problem of the nonhomogeneous environment and large computation burden of fully adaptive space time processing, some typical suboptimal STAP approaches were proposed [31–37]. In the end of 1990s, the knowledge-based space-time adaptive processing (KB-STAP) for airborne early warning radar was proposed, which was the hot topic in the first ten years of the 21st century [38–40]. However, the STAP's performance becomes significantly degradation when the target and clutter are similar to each other in the angle domain and Doppler domain or when the knowledges do not agree with the reality in KB-STAP.

Traditionally, the significant attention on clutter suppression has been given to one- and two-domain processing. However, as the difference between the target and clutter in one- or two-domain may be very small, the performance of the processing is degraded. The adaptive polarization-space-time joint domain processing for radar target detection in nonhomogeneous or nonstationary clutter environments were developed by Park [41–43] et al. in 1990s. Properties of the degree of cross-polarization in the space-time domain were analyzed in [44]. However, the factors which effect on the performance of clutter suppression are not clear. As a result, some new techniques (i.e., covariance matrix eigendecomposition spectral analysis and resolution grid processing method) are utilized for deriving performance of clutter suppression in polarization-space-time joint domain processing (PST-JDP).

This paper is organized as follows. We firstly formulate the received signal model of PST-JDP in Section 2. In Section 3 we

propose a new method to analyse optimum PST-JDP. Compared to STAP's performance, we analyze the performance superiority of PST-JDP. Experimental results and discussions are shown in Section 4. Finally, Section 5 summarizes the conclusions.

2. FUNDAMENTALS OF PST-JDP

2.1. Signal Model

The radar antenna system that consists of N-element uniform linear array (ULA) is considered. Each element consists of two-dipole which is sensitive to the echo polarization diversity. One is horizontally polarized and the other is vertically polarized. The array consists of H channel subarray which contains N horizontally polarized sensors and V channel subarray which contains N vertically polarized sensors. The two subarrays are assumed to have the same array geometry as shown in Figure 2(a). Assume S_i is the ith target scatter point φ denotes the azimuth angle of the signal source with $0 \leq \varphi \leq \pi$, and θ denotes the elevation angle of the signal source with $0 \leq \theta \leq \pi/2$. The radar echo is assumed to be a burst of M identical pulses with PRF in a coherent processing interval (CPI). The received signal which is down-converted and matched filtered to produce a baseband signal may be written as

$$\mathbf{x} = \boldsymbol{\alpha}_0 \mathbf{v}_0 + \mathbf{x}_c + \mathbf{x}_n \tag{1}$$

where $\boldsymbol{\alpha}_0$ is the unknown complex constant representing the amplitude and phase of a target return and $\mathbf{v}_0$ the signal polarization-space-time joint steering vector of a known form. $\mathbf{x}_c$ and $\mathbf{x}_n$ are the $2MN$-by-1 clutter and noise vector, respectively. For simplicity of discussion

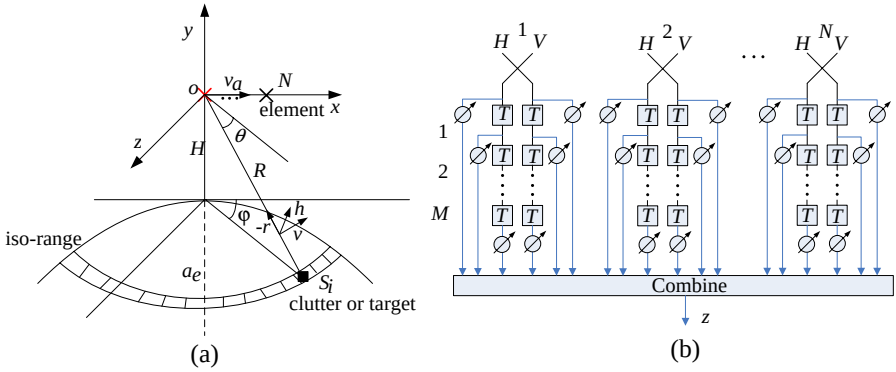

Figure 2. (a) Polarization sensitive array and clutter/target scatter geometry distribution. (b) Optimum PST-JDP signal processing chart.

only, we assume that the spatial elements are colinear, identical, omni-directional, and equally spaced with spacing d. The polarization-space-time joint steering vector ($2MN$-by-1) can be written as follows

$$\mathbf{v}_0 = \mathbf{v}_p(\gamma,\eta) \otimes \mathbf{v}_t(f_d) \otimes \mathbf{v}_s(f_s) \tag{2}$$

where $\otimes$ denotes the Kronecker product $\mathbf{v}_p(\gamma,\eta)$, $\mathbf{v}_t(f_d)$ and $\mathbf{v}_s(f_s)$ denote the corresponding polarization, Doppler and space steering vectors, respectively. $\mathbf{v}_p(\gamma,\eta)$ has the expression

$$\mathbf{v}_p(\gamma,\eta) = \begin{bmatrix} \cos\gamma \\ \sin\gamma\exp(j\eta) \end{bmatrix} \tag{3}$$

where γ and η denote the amplitude ratio and phase difference between two channels, respectively. $\mathbf{v}_t(f_d)$ has the expression

$$\mathbf{v}_t(f_d) = [1 \quad \exp(j2\pi f_d) \quad \ldots \quad \exp(j2\pi(M-1)f_d)]^T \tag{4}$$

where $(\cdot)^T$ denotes vector transposition. f_d is target normalized Doppler frequency with $f_d = \frac{2v_a}{\lambda_0 PRF}\cos\theta\cos\varphi + \frac{2v_r(S_0)}{\lambda_0 PRF}$, v_a the airborne platform velocity, v_r the ith target radial velocity, and λ_0 the radar wavelength $\mathbf{v}_s(f_s)$ has the expression

$$\mathbf{v}_s(f_s) = [1 \quad \exp(j2\pi f_s) \quad \ldots \quad \exp(j2\pi(N-1)f_s)]^T \tag{5}$$

where f_s is the target spatial frequency with $f_s = \frac{d\cos\theta\cos\varphi}{\lambda_0}$.

Unlike a target, the ground/sea clutter is distributed in all range and all azimuths and is spread in Doppler frequency due to the radar platform motion. We use the standard space-time clutter model for a uniform linear array which was codified in Ward's oft-cited report [32] and combined polarization-space-time covariance matrix by Park [41]. Modified clutter covariance matrix (CCM) is written as

$$\mathbf{R}_{pst}^{(c)} = E\left\{\mathbf{x}_c\mathbf{x}_c^H\right\} = \bar{\mathbf{R}}_p \otimes \mathbf{R}_{s-t} \tag{6}$$

where $\bar{\mathbf{R}}_p$ is the normalized polarization covariance matrix and denotes polarization correlation characteristic, which can be written as

$$\bar{\mathbf{R}}_p = \frac{1}{1+r}\begin{bmatrix} 1 & \sqrt{r}\,|\mu|\,e^{-j\bar{\phi}} \\ \sqrt{r}\,|\mu|\,e^{j\bar{\phi}} & r \end{bmatrix} \tag{7}$$

where r is the power ratio between H channel and V channel, μ the complex correlation coefficient between the two channels, $\bar{\phi} = \arg(\mu)$ the statistical average phase difference, and $\arg(\cdot)$ returns the phase angles.

The clutter degree of polarization (DP) can be defined in terms of the elements of covariance matrix, which is given by

$$\rho = \sqrt{1 - \frac{4\det\bar{\mathbf{R}}_p}{(\mathrm{Tr}\bar{\mathbf{R}}_p)^2}} = \sqrt{1 - \frac{4r(1-|\mu|^2)}{(1+r)^2}} \tag{8}$$

If power ratio is unit, clutter degree of polarization equals to the absolute value of complex correlation coefficient, $\rho = |\mu|$. $\mathbf{R}_{s-t}$ is the space-time clutter covariance matrix and denotes spatial and temporal correlation, which can be written as

$$\mathbf{R}_{s-t} = \sum_{i=1}^{N_c} \left\{ \gamma(S_i) \mathbf{v}_t \left(f_d^{(i)} \right) \mathbf{v}_t^H \left(f_d^{(i)} \right) \otimes \mathbf{v}_s \left(f_s^{(i)} \right) \mathbf{v}_s^H \left(f_s^{(i)} \right) \right\} \quad (9)$$

where N_c is number of independent clutter patches evenly distributed in azimuth about the radar, $\gamma(S_i)$ the power of the ith clutter patch, and $f_d^{(i)}$ and $f_s^{(i)}$ denote the normalized Doppler frequency and spatial frequency of ith clutter patch, respectively.

The covariance matrix of receiver noise is addressed as follows. The receiver noise output from the subarrays is assumed to be zero mean Gaussian random variables, independent, identically distributed, and independent of clutter. The covariance matrix of noise is $\sigma^2 \mathbf{I}_{2MN}$ with zero mean, where σ^2 denotes noise power and $\mathbf{I}_{2MN}$ denotes $2MN \times 2MN$ dimensional unity diagonal matrix. The total clutter plus noise polarization-space-time covariance matrix, denoted by $\mathbf{R}_{c+n}$, can be written as a linear combination of $\mathbf{R}_{pst}^{(c)}$ and $\sigma^2 \mathbf{I}_{2MN}$, which is

$$\mathbf{R}_{c+n} = \mathbf{R}_{pst}^{(c)} + \sigma^2 \mathbf{I}_{2MN} = \bar{\mathbf{R}}_p \otimes \mathbf{R}_{s-t} + \sigma^2 \mathbf{I}_{2MN} \quad (10)$$

2.2. Optimum PST-JDP

Figure 2(b) shows the optimum PST-JDP chart. The target polarization-space-time steering vector $\mathbf{v}_0$ and $2MN \times 2MN$ clutter plus noise covariance matrix $\mathbf{R}_{c+n}$ are given in Figure 2(b). It is well known that the optimal weight of the $2MN$-length data vector which maximizes the output signaltointerferenceplusnoise ratio (SINR) can be written as

$$\mathbf{w} = \mathbf{R}_{c+n}^{-1} \mathbf{v}_0 \quad (11)$$

and the corresponding output SINR is

$$SINR_{\max}^{(pst)} = P_s \mathbf{v}_0^H \mathbf{R}_{c+n}^{-1} \mathbf{v}_0 = SNR_{in} \sigma^2 \mathbf{v}_0^H \mathbf{R}_{c+n}^{-1} \mathbf{v}_0 \quad (12)$$

where P_s is the desired signal power, $P_s = E[|\boldsymbol{\alpha}_0|^2]$, and SNR_{in} denotes the received signal-to-noise ratio of a single element and single pulse. SNR_{in} Polarized sensitive array processing gain is defined as

$$SNR_{gain} = \frac{SINR_{\max}^{(pst)}}{SNR_{in}} = \sigma^2 \mathbf{v}_0^H \mathbf{R}_{c+n}^{-1} \mathbf{v}_0 \quad (13)$$

3. A NEW METHOD FOR OPTIMUM PST-JDP

From (10), $\bar{\mathbf{R}}_p$ and $\mathbf{R}_{s-t}$ denote polarization and space-time covariance matrix (CM), respectively. $\bar{\mathbf{R}}_p$ and $\mathbf{R}_{s-t}$ are Hermitian matrix, which play a central role in performance analysis in this section.

3.1. Polarization CM Eigendecomposition

Since $\bar{\mathbf{R}}_p$ is a Hermitian matrix, its eigenvalues are real and corresponding eigenvectors are orthogonal with each other. In particular, one partially polarized wave can decompose two completely polarized waves which are orthogonal with each other. Thus Eq. (7) can be decomposed as

$$\bar{\mathbf{R}}_p = \lambda_1 \boldsymbol{\alpha}_1 \boldsymbol{\alpha}_1^H + \lambda_2 \boldsymbol{\alpha}_2 \boldsymbol{\alpha}_2^H \tag{14}$$

where $\lambda_i (i = 1, 2)$ is the ith descending-ordered eigenvalue of $\bar{\mathbf{R}}_p$ and $\boldsymbol{\alpha}_i$ $(i = 1, 2)$ the corresponding eigenvector. $\boldsymbol{\alpha}_1$ is defined as the main polarized vector which denotes the position on Poincare sphere. $\boldsymbol{\alpha}_2$ is the secondary polarized vector which denotes the position on Poincare sphere as well. The eigenvalues and eigenvectors can be written in detail as

$$\begin{aligned} \lambda_1 &= \frac{(1+\rho)}{2}, \quad \boldsymbol{\alpha}_1 = k_1 \begin{bmatrix} r-1-(1+r)\rho \\ -2\sqrt{r}\,|\mu|\, e^{j\bar{\phi}} \end{bmatrix} \\ \lambda_2 &= \frac{(1-\rho)}{2}, \quad \boldsymbol{\alpha}_2 = k_2 \begin{bmatrix} r-1+(1+r)\rho \\ -2\sqrt{r}\,|\mu|\, e^{j\bar{\phi}} \end{bmatrix} \end{aligned} \tag{15}$$

where k_1 and k_2 are normalized coefficient, $\boldsymbol{\alpha}_1^H \boldsymbol{\alpha}_1 = \boldsymbol{\alpha}_2^H \boldsymbol{\alpha}_2 = 1$, and $\boldsymbol{\alpha}_1^H \boldsymbol{\alpha}_2 = \boldsymbol{\alpha}_2^H \boldsymbol{\alpha}_1 = 0$. The partially polarized wave can be decomposed as two orthogonal completely polarized waves, which can be described through the Stokes vector $\mathbf{g}$, whose components are defined as follows

$$\mathbf{g} = \begin{bmatrix} g_0 \\ g_1 \\ g_2 \\ g_3 \end{bmatrix} = \begin{bmatrix} 1 \\ |\boldsymbol{\alpha}_i(1)|^2 - |\boldsymbol{\alpha}_i(2)|^2 \\ 2\,|\boldsymbol{\alpha}_i(1)|\,|\boldsymbol{\alpha}_i(2)| \cos\phi_i \\ 2\,|\boldsymbol{\alpha}_i(1)|\,|\boldsymbol{\alpha}_i(2)| \sin\phi_i \end{bmatrix} \quad i = 1, 2 \tag{16}$$

where ϕ_i is the phase difference between two channels, and $\phi_i = \arg(\boldsymbol{\alpha}_i(2)/\boldsymbol{\alpha}_i(1))$. Defined γ_i as amplitude ratio, $\gamma_i = \tan^{-1}(|\boldsymbol{\alpha}_i(2)| \,/\, |\boldsymbol{\alpha}_i(1)|)$. For $\boldsymbol{\alpha}_1$ is orthogonal with $\boldsymbol{\alpha}_2$, we have $\phi_1 - \phi_2 = \pm\pi$ and $\gamma_1 + \gamma_2 = \pi/2$. By the representation of Poincare sphere [5], any polarization state of a completely polarized wave can be represented by a point $\mathbf{S}$ with Cartesian co-ordinates which are expressed through Stokes parameters as follows

$$\mathbf{S} = \begin{pmatrix} g_1 & g_2 & g_3 \end{pmatrix} \tag{17}$$

Because the wave is supposed to be completely polarized, polarizations are mapped on to the surface of sphere (seen in Figure 3). The extremum of each diameter corresponds to a pair of orthogonal polarizations, which may denote the main polarization vector and secondary polarization vector.

3.2. Spacetime CM Eigendecomposition

Spacetime CM is a Hermitian matrix, which can be decomposed as

$$\mathbf{R}_{s-t}\boldsymbol{\beta}_j = \mu_j \boldsymbol{\beta}_j \tag{18}$$

where μ_j and $\boldsymbol{\beta}_j$ are the eigenvalue and eigenvector of space time covariance matrix $\mathbf{R}_{s-t}$, respectively. Slepian and Pollak [45, 46] and Fancourt and Principe [47] demonstrated some asymptotic relationship in the eigenvalues, eigenfunctions, and PSD of the random process. For the clutter power spectral density (PSD) $P(f_s, f_d)$ are the 2D Fourier transform (FT) of covariance matrix $\mathbf{R}_{s-t}$, we have

$$P(f_s, f_d) = \sum_{i=1}^{N_c} \gamma(S_i)\delta\left(f_s - f_s^{(i)}\right)\delta\left(f_d - f_d^{(i)}\right) \tag{19}$$

where $f_d^{(i)} = \beta f_s^{(i)}$, β is the slope of clutter ridge, as shown $\beta = \frac{2v_a}{dPRF}$. It is clear that this curve is precisely the 2D direction Doppler curve (DDC). Hence, the 2D DDC is the support of the clutter PSD. The clutter energy is distributed in 2D angle-Doppler curve (i.e., the ridge of the clutter) (seen in Figure 3 and Figure 4). According to the relationship between eigenvalue of space-time CM and PSD [40], the

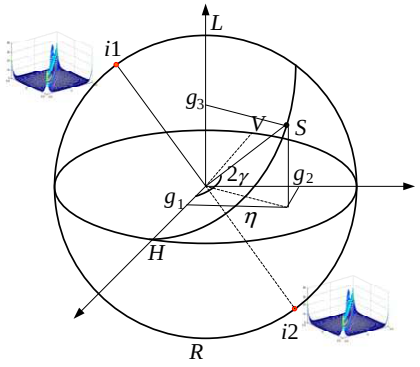

Figure 3. Polarization position on Poincare sphere.

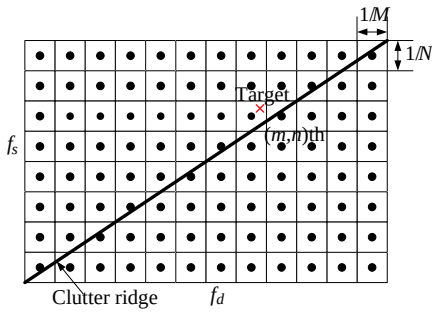

Figure 4. Resolution grids.

eigenvalue of $\mathbf{R}_{s-t}$ can be written as

$$\mu_j \approx \frac{1}{A_g} \iint\limits_{G_j} P(f_s, f_d) df_s df_d \tag{20}$$

where G_j is the jth resolution grid (a rectangular region with $[f_d - 1/2M, f_d + 1/2M] \times [f_s - 1/2N, f_s + 1/2N]$) on the angle-Doppler plane and $A_g = 1/(MN)$ the size of the grid G_j. As shown in Figure 4, the angle-Doppler plane can be sliced into many resolution grids and each grid corresponds to an eigenvalue. Centre frequency of each grid corresponding to Fourier basis of eigenvector can be written as

$$\boldsymbol{\beta}_j = e^{j2\pi f_{m,n}} \tag{21}$$

where $f_{m,n} = (m/M, n/N)$ is the centre frequency of the (m, n)th grid.

3.3. Polarizationspacetime CM Eigendecomposition

Theorem 1: Given the matrix $\mathbf{R}_{c+n} = \bar{\mathbf{R}}_p \otimes \mathbf{R}_{s-t} + \sigma^2 \mathbf{I}_{2MN}$. If λ_i and $\boldsymbol{\alpha}_i$ are respectively the eigenvalue and eigenvector of matrix $\bar{\mathbf{R}}_p$, and μ_j and $\boldsymbol{\beta}_j$ are respectively the eigenvalue and eigenvector of matrix $\mathbf{R}_{s-t}$ $\boldsymbol{\alpha}_i \otimes \boldsymbol{\beta}_j$ is the eigenvector of matrix $\bar{\mathbf{R}}_p \otimes \mathbf{R}_{s-t}$ and the corresponding eigenvalue is $\lambda_i \mu_j$.

Corollary 1: $\boldsymbol{\alpha}_i \otimes \boldsymbol{\beta}_j$ is also the eigenvector of matrix $\mathbf{R}_{c+n} = \bar{\mathbf{R}}_p \otimes \mathbf{R}_{s-t} + \sigma^2 \mathbf{I}_{2MN}$, and the corresponding eigenvalue is $\lambda_i \mu_j + \sigma^2$.

4. PERFORMANCE ANALYSIS

4.1. Performance Analysis of PST-JDP

According to Theorem 1 and Corollary 1, the polarization array processing gain SNR_{gain} can be decomposed as

$$SNR_{gain} = \sum_{i=1}^{2} \sum_{j}^{MN} \frac{\sigma^2 \left| \mathbf{v}_{ij}^H \mathbf{v}_0 \right|^2}{\lambda_c^{(ij)} + \sigma^2} \tag{22}$$

where $\lambda_c^{(ij)} = \lambda_i \mu_j$ denotes PSD of ith polarized position of Poincare and jth resolution grid, center frequency of jth resolution grid $f_{m,n} = (m/M, n/N)$, when $M \to \infty$ and $N \to \infty$. Thus, the corresponding polarization-space-time joint steering vector of $\lambda_c^{(ij)}$ is

$$\mathbf{v}_{ij} = \boldsymbol{\alpha}_i \otimes \mathbf{v}_{s-t}(f_{m,n}) = \boldsymbol{\alpha}_i \otimes \mathbf{v}_{s-t}(m/M, n/N) \tag{23}$$

(22) may also be written as

$$SNR_{gain} = \sum_{i=1}^{2}\sum_{m=1}^{M}\sum_{n}^{N}\frac{\sigma^2\left|\left(\boldsymbol{\alpha}_i^H \otimes \mathbf{v}_{s-t}^{(m,n)H}\right)\mathbf{v}_0\right|^2}{\lambda_c^{(i,m,n)}+\sigma^2} = \sum_{i=1}^{2}\sum_{m=1}^{M}\sum_{n}^{N}\frac{\sigma^2\chi_{i,m,n}}{\lambda_c^{(i,m,n)}+\sigma^2} \tag{24}$$

where $\lambda_c^{(i,m,n)}$ is equal to $\lambda_c^{(ij)}$, which denotes the power spectra of the ith polarized position of Poincare and the (m,n)th resolution grid. $\chi_{i,m,n}$ is defined as the inner of steering vector, which can be written as

$$\chi_{i,m,n} = \left|\boldsymbol{\alpha}_i^H\boldsymbol{\alpha}_0\right|^2\left(\frac{\sin\left[N\pi(f_{s0}-n/N)\right]}{\sin\left[\pi(f_{s0}-n/N)\right]}\frac{\sin\left[M\pi(f_{d0}-m/M)\right]}{\sin\left[\pi(f_{d0}-m/M)\right]}\right)^2 \tag{25}$$

where $\boldsymbol{\alpha}_0$, f_{s0}, and f_{d0} denote polarization, spatial frequency and Doppler frequency of the target, respectively. If the target spatial and temporal frequency is not in the (m,n)th grid, $\chi_{i,m,n}$ is very small. Therefore, the SNR gain is mainly due to the grid of target. Assume it is in the (k,l)th grid, (24) can be written as

$$SNR_{gain} = \sum_{i=1}^{2}\frac{\sigma^2\chi_{i,k,l}}{\lambda_c^{(i,k,l)}+\sigma^2} = \sum_{i=1}^{2}\frac{\sigma^2\left|\boldsymbol{\alpha}_i^H\boldsymbol{\alpha}_0\right|^2}{\lambda_i\mu_{k,l}+\sigma^2}\chi_{k,l} \tag{26}$$

where $\mu_{k,l}$ is the PSD of clutter in the (k,l) grid, and $\chi_{k,l}$ denotes the spatial and temporal gain of the target, which may be written as

$$\chi_{k,l} = \left(\frac{\sin\left[N\pi(f_{s0}-k/N)\right]}{\sin\left[\pi(f_{s0}-k/N)\right]}\frac{\sin\left[M\pi(f_{d0}-l/M)\right]}{\sin\left[\pi(f_{d0}-l/M)\right]}\right)^2 \tag{27}$$

If Doppler frequency of a target is large and clutter does not exist in the resolution grid of the target, (i.e., $\mu_{k,l} \approx 0$), Eq. (26) is also expressed as

$$SNR_{gain} = \chi_{k,l}\left(\left|\boldsymbol{\alpha}_1^H\boldsymbol{\alpha}_0\right|^2 + \left|\boldsymbol{\alpha}_2^H\boldsymbol{\alpha}_0\right|^2\right) = \chi_{k,l} \tag{28}$$

If clutter exists, the angle between polarization steering vector of target and main polarization vector of clutter (AP) is assumed as α with $0 \le \alpha \le \frac{\pi}{2}$ as shown in Figure 5. α is defined as the wide polarization distance in polarization domain. We can rewrite Eq. (26)

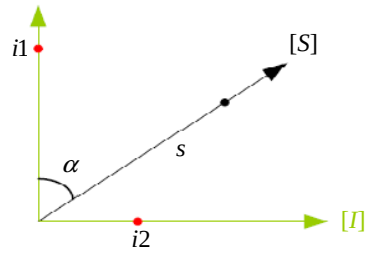

Figure 5. Angle between target and clutter in polarization domain.

as

$$SNR_{gain} = \sigma^2 \chi_{k,l} \left[\left(\frac{\left| \boldsymbol{\alpha}_1^H \boldsymbol{\alpha}_0 \right|^2}{\lambda_1 \mu_{k,l} + \sigma^2} + \frac{\left| \boldsymbol{\alpha}_2^H \boldsymbol{\alpha}_0 \right|^2}{\lambda_2 \mu_{k,l} + \sigma^2} \right) \right]$$
$$= \sigma^2 \chi_{k,l} \left[\frac{\cos^2 \alpha}{\frac{1+\rho}{2} \mu_{k,l} + \sigma^2} + \frac{\sin^2 \alpha}{\frac{1-\rho}{2} \mu_{k,l} + \sigma^2} \right] \tag{29}$$

where

$$\alpha = \arccos \frac{\left| \langle \boldsymbol{\alpha}_0, \boldsymbol{\alpha}_1 \rangle \right|}{\|\boldsymbol{\alpha}_0\| \, \|\boldsymbol{\alpha}_1\|} = \arccos \left| \langle \boldsymbol{\alpha}_0, \boldsymbol{\alpha}_1 \rangle \right| \tag{30}$$

Given the above deducibility, (12) can also be written as

$$SINR_{\max}^{(pst)} \approx SNR_{in} \sigma^2 \cdot \chi_{k,l} \left[\frac{\cos^2 \alpha}{\frac{1+\rho}{2} \mu_{k,l} + \sigma^2} + \frac{\sin^2 \alpha}{\frac{1-\rho}{2} \mu_{k,l} + \sigma^2} \right] \tag{31}$$

From Eqs. (28) and (31), we can deduce that the maximum output SINR depends on the input SNR, clutter PSD in the target grid (or CNR), polarization distance clutter degree of polarization, target Doppler and spatial frequency. According to (31), the larger is the polarization distance and the higher is the clutter degree of polarization, the bigger is the output SINR.

4.2. Compared to STAP's Performance

We have studied the clutter suppression performance of PST-JDP. The output SINR in the case of STAP is

$$SINR_{\max}^{(st)} \approx SNR_{in} \sigma^2 \cdot \chi_{k,l} \cdot \frac{1}{\mu_{k,l} + \sigma^2} \tag{32}$$

where $SINR_{\max}^{(st)}$ denotes the output SINR for STAP method. Then, the right part of Eq. (32) may be written as

$$\begin{aligned} & SNR_{in}\sigma^2 \cdot \chi_{k,l} \cdot \frac{1}{\mu_{k,l}+\sigma^2} \\ &= SNR_{in}\sigma^2 \cdot \chi_{k,l} \cdot \frac{\sin^2\alpha+\cos^2\alpha}{\mu_{k,l}+\sigma^2} \\ &= SNR_{in}\sigma^2 \cdot \chi_{k,l} \cdot \left[\frac{\sin^2\alpha}{\mu_{k,l}+\sigma^2}+\frac{\cos^2\alpha}{\mu_{k,l}+\sigma^2}\right] \\ &\le SNR_{in}\sigma^2 \cdot \chi_{k,l} \cdot \left[\frac{\cos^2\alpha}{\frac{1+\rho}{2}\mu_{k,l}+\sigma^2}+\frac{\sin^2\alpha}{\frac{1-\rho}{2}\mu_{k,l}+\sigma^2}\right] \\ &= SINR_{\max}^{(pst)} \end{aligned} \tag{33}$$

So far, we have analyzed that the performance of PST-JDP is better than STAP theoretically.

5. EXPERIMENTAL RESULTS AND DISCUSSIONS

The SINR loss of a processing algorithm is defined to be output SINR in the case of interference/clutter relative to the matched filter SNR in an interference-free environment [32], which is

$$L_{SINR} = 10\log_{10}(SINR_{\max}/SNR_o) = 10\log_{10}(SNR_{gain}/MN) \tag{34}$$

Table 1. System parameters.

Parameter	Symbol	value
Number of sensors	N	8
Number of pulses	M	12
Radar wavelength	λ_0	0.3 m
Inter-sensor spacing	d	0.15 m
Pulse repetition interval	PRI	5 ms
Clutter-to-noise ratio	CNR	30 dB
Signal-to-noise ratio	SNR	0 dB
Azimuth angle	φ	[0°, 180°]
Platform velocity	v_a	150 m/s
Clutter degree of polarization	ρ	0.999
Clutter statistical average phase difference	$\bar{\phi}$	90°

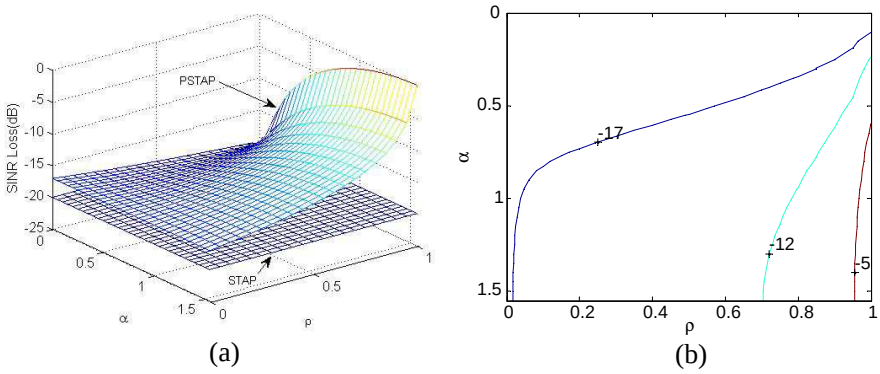

(a) (b)

Figure 6. (a) SINR loss versus AP and DP in the case of PST-JDP by theory method. (b) Contour figure for SINR loss versus AP and DP in the case of PST-JDP by theoretical method.

where $SNR_o = MN \cdot SNR_{in}$ is the optimum matched filter output signal-to-noise ratio in absence of clutter. SINR loss is useful because the performance metric is independent on the input signal power. The processor performance can be translated to a radar system's detection performance by including it as an additional loss factor in the radar equation. If $L_{SINR} = -5\,\text{dB}$, the radar detection range after a processor is 75% of the radar's noise-limited detection range at least. Similarly, if $L_{SINR} = -12\,\text{dB}$ at least 50% of the radar's maximum detection range is acceptablely defined. In the next simulation, the airborne platform is side-looking ULA. Some typical system parameters are listed in Table 1.

5.1. Effect of AP and DP

Figure 6 and Figure 7 show the effects of DP and AP on SINR loss. Figure 6 depicts the theoretical analyses results by Eqs. (29), (32), and (34). Figure 7 gives the simulation results by Eqs. (13) and (34). For Figure 6, assume that the range of clutter degree of polarization is $0 \leq \rho \leq 1$ and that the angle of between target polarization steering vector and clutter main polarization vector is $0 \leq \alpha \leq \pi/2$. The received thermal noise power is 1 and the clutter-and-noise ration is 20 dB in the grid of target. Figure 6(a) shows that the performance of clutter suppression becomes better for PST-JDP when the clutter degree of polarization is higher and the polarization angle between then target and main clutter is larger. The SINR loss for STAP is $-20.04\,\text{dB}$ which demonstrates that the performance of clutter suppression for

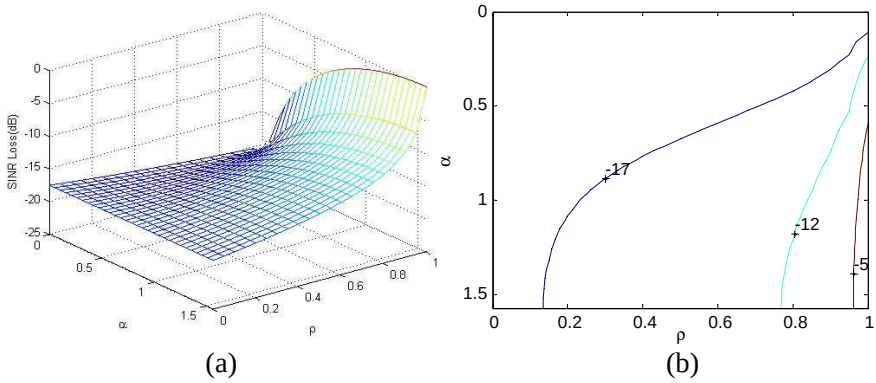

Figure 7. (a) SINR loss versus AP and DP in the case of PST-JDP by simulation method. (b) Contour figure for SINR loss versus AP and DP in the case of PST-JDP by simulation method.

PST-JDP in the case of slowly moving target is significantly superior to the performance of STAP. Figure 6(b) is the contour figure of Figure 6(a) and shows that the radar detection range for PST-JDP algorithm is at least 75% of the radar's noise-limited detection range with $0.95 \leq \rho \leq 1$ and $0.58 \leq \alpha \leq 1.73$ in the scene. Similarly, it is about 50% of the radar's noise-limited detection range in the case of $0.7 \leq \rho \leq 1$ and $0.24 \leq \alpha \leq 1.73$. However, the radar for STAP algorithm can't detect target if clutter is present in the grid of target. Figure 6(b) also shows that the clutter polarization degree is the main factor to effect on the performance of clutter suppression. The total clutter-and-noise ratio is assumed to be 23 dB in Figure 7, because the accurate CNR value in the grid of target is not known. The simulative results are similar to the theoretical results, which demonstrate the theoretical analyses correctness.

5.2. Effect of Doppler and DP

Figure 8 shows that the eigenspectra of clutter versus the clutter polarization degree, with $\rho = 0.999$, $\rho = 0.99$, and $\rho = 0.9$. In Figure 8, the number of big eigenvalue increases as the clutter polarization degree becomes small. From Eq. (22), the results will be demonstrated. The big eigenvalue number of clutter polarization-space-time covariance matrix is is not less than the big eigenvalue number of clutter space-time covariance matrix and not more than the twice of big eigenvalue of space-time algorithm. For Figure 8,

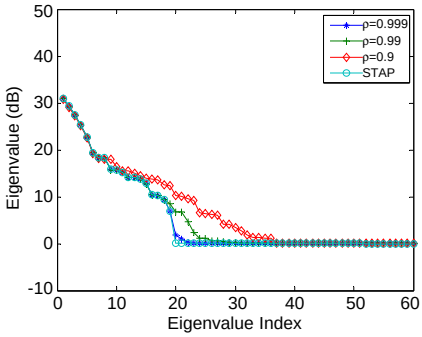

Figure 8. Eigenspectra versus clutter polarization degree, $\rho = 0.999$, $\rho = 0.99$, $\rho = 0.9$.

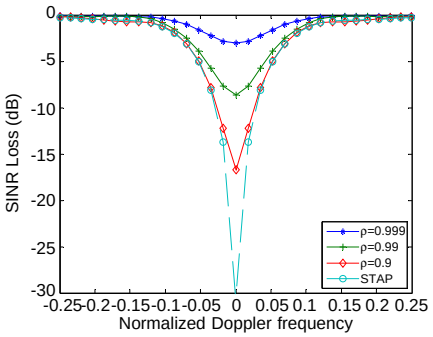

Figure 9. SINR loss versus target Doppler frequency in the case of different clutter polarization degree for PST-JDP method, $\rho = 0.999$, $\rho = 0.99$, $\rho = 0.9$, and SINR loss versus target Doppler frequency for STAP method.

according to Brennan's rule, eight elements and twelve coherent pulses are assumed in the case of a narrowband N element ULA with half of wavelength inter element spacing, in the absence of antenna crabbing. Assumming M coherent processing pulses are received, the clutter rank K is approximately given by $K = \lceil N + \beta(M-1) \rceil$ [28], where β is the slope of clutter ridge and $\lceil\ \rceil$ denotes the "ceiling" operator. According to eigenvalue discomposition, the big eigenvalue of polarization-space-time covariance matrix (PST-CM) is $\lceil N + \beta(M-1) \rceil \leq K' \leq 2\lceil N + \beta(M-1) \rceil$. The big eigenvalue number is more than 19 and less than 38. When the clutter is completely polarized wave, the big eigenvalue number of PST-CM is $K' = \lceil N + \beta(M-1) \rceil$.

Figure 9 shows the effect of normalized Doppler frequency and clutter degree of polarization on SINR loss in the case of PST-JDP, SINR loss versus target Doppler frequency for STAP method. For Figure 9, target polarization phase difference is $-60°$, clutter is circular polarization and the clutter average phase difference $\bar{\phi} = 90°$. From Figure 9, the performance of PST-JDP and STAP becomes worse when the normalized target Doppler frequency is smaller. However, when the clutter degree of polarization is higher, the performance of PST-JDP is also good, which verifies the performance of PST-JDP is obviously better than the performance of STAP, especially when the target is slowly moving. The minimum SINR loss is $-4.3\,\mathrm{dB}$ with $\rho = 0.999$, which means that the radar detection range in the scene is more

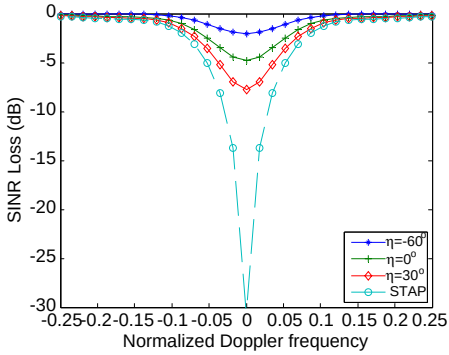

Figure 10. SINR loss versus target Doppler frequency in the case of different target phase difference for PST-JDP method, $\eta = -60°$, $\eta = 0°$, $\eta = 30°$, and SINR loss versus target Doppler frequency for STAP method.

than 75% of the radar's noise-limited detection range. However, when the DP is low, the performance of PST-JDP becomes worse because random clutter on Poincare sphere is difficult to suppress. When the normalized Doppler frequency is large, the performance of PST-JDP is similar to the performance of STAP.

5.3. Effect of Doppler and AP

Figure 10 shows SINR loss versus target Doppler frequency in the case of different target phase difference for PST-JDP method, $\eta = -60°$, $\eta = 0°$, $\eta = 30°$, and SINR loss versus target Doppler frequency for STAP method. For Figure 10, the clutter degree of polarization is $\rho = 0.999$ and the clutter average phase difference is $\bar{\phi} = 90°$. From Figure 10, when normalized target Doppler frequency becomes smaller, the performance of PST-JDP and STAP becomes worse. However, the performance of PST-JDP is also good when the polarization difference between the target and clutter is large. The reason is that the polarization information in PST-JDP algorithm is used to discriminate the target and clutter. In all scene of PST-JDP, the SINR loss is more than -12 dB, which means that the radar detection range is more than 50% of the radar's noise-limited detection range. However, detection range of STAP algorithm is poor when the target normalized Doppler frequency is low.

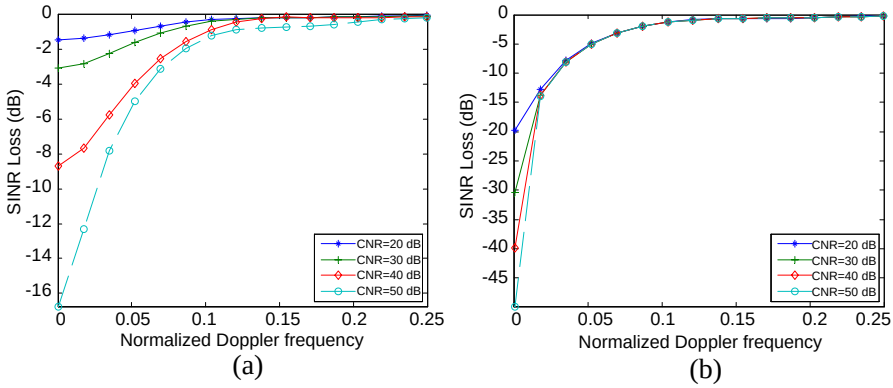

Figure 11. (a) SINR loss versus target normalized Doppler frequency in the case of different CNR for PST-JDP method. (b) SINR loss versus target normalized Doppler frequency in the case of different CNR for STAP method, $CNR = 20\,\text{dB}$, $30\,\text{dB}$, $40\,\text{dB}$, $50\,\text{dB}$.

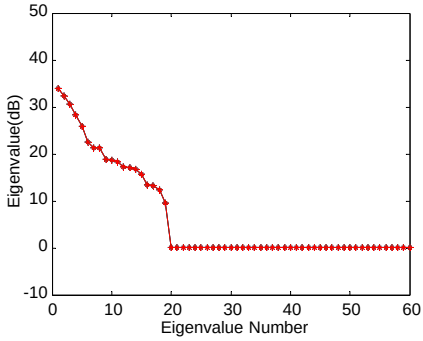

Figure 12. Eigenspectra in completely polarized wave.

5.4. Effect of CNR

Figure 11 shows SINR loss versus target normalized Doppler frequency in the case of different CNR for PST-JDP method and for STAP method, respectively. For Figure 11(a), the target polarization phase difference between two channels is $\eta = -30°$, the clutter degree of polarization is $\rho = 0.999$ and the clutter average phase difference is $\bar{\phi} = 90°$. The SINR loss becomes lower as the CNR becomes larger in Figure 11(a), when the target is slowly moving. However, when the CNR is less than 40 dB in the scene, the SINR loss is more than $-12\,\text{dB}$, which means that the radar detection range is more than 50% of the radar's noise-limited detection range. For Figure 11(b), the SINR loss

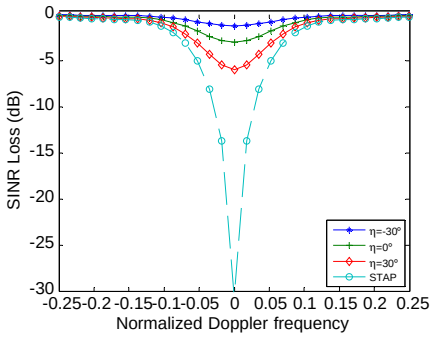

Figure 13. SINR loss versus target Doppler frequency in the case of different target phase difference for PST-JDP method, $\eta = -30°$, $\eta = 0°$, $\eta = 30°$, clutter is completely polarized.

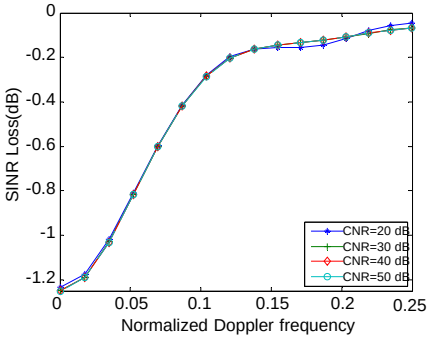

Figure 14. SINR loss versus target normalized Doppler frequency in the case of different CNR for PST-JDP method, $CNR = 20\,\text{dB}$, 30 dB, 40 dB, 50 dB, $\eta = -30°$.

of STAP descends significantly as the CNR increases in the case of target slow moving. The SINR loss is approximately inverse ratio to value of CNR. From Figure 11, the effect of CNR on the performance of clutter suppression is small when the target normalized Doppler frequency is large.

5.5. Assumed Clutter as Completely Polarized Wave

In this section, the clutter is assumed as completely polarization wave. Figure 12 shows the number of big eigenvalue in the case of completely polarized wave. The big eigenvalue number of clutter polarization-space-time covariance matrix is 19 and is equal to the big eigenvalue number of clutter space-time covariance matrix. From (22), the results may be demonstrated. This means that clutter degree of free is not various for optimum PST-JDP and equals to DOF of space-time processing method when the clutter is completely polarized. The degree of freedom (DOF) of system for optimum PST-JDP method is twice bigger than optimum space-time processing method. Therefore, the performance for clutter suppression by optimum PST-JDP method is superior to space-time processing method.

Figure 13 shows SINR loss varies with the target Doppler frequency in the case of different target phase difference for PST-JDP and STAP methods, when $\eta = -30°$, $\eta = 0°$, and $\eta = 30°$, with completely polarized clutter. Compared to Figure 10, the performance

for PST-JDP method in the case of completely polarized wave is superior to the partially polarized wave.

Figure 14 shows SINR loss versus target normalized Doppler frequency in the case of different CNR for PST-JDP method in the case of completely polarized wave, when $CNR = 20\,\text{dB}, 30\,\text{dB}, 40\,\text{dB}, 50\,\text{dB}$ and $\eta = -30^\circ$. For Figure 14, CNR is small to effect on performance in the case of completely polarized wave.

6. CONCLUSIONS

In this study, some new methods (i.e., eigendecomposition, spectral analysis and resolution grid) are utilized for deriving performance of clutter suppression by optimal polarization-space-time joint domain processing (PST-JDP) technique. We demonstrated that the performance of clutter suppression depends on DP, AP, input CNR Doppler frequency. Several simulative results confirmed the validity of the theoretical works and shown that the proposed method can provide robustness performance. The details of results are as follows:

(i) The optimal PST-JDP for clutter suppression is superior to optimal space-time processing, especially when target is slowly or tangentially moving. As the spatial frequency and Doppler frequency between target and clutter are similar, optimal PST-JDP technology can discriminate target and clutter by polarization characteristic difference and suppress the clutter.

(ii) The optimum PST-JDP is sensitive to polarization characteristic of clutter (i.e., clutter degree of polarization) and the polarization difference between target and clutter. Clutter degree of polarization is the main factor to effect on the performance for clutter suppression. The performance of clutter suppression becomes better as the clutter polarization degree becomes higher and the polarization difference between target and clutter becomes larger.

(iii) When the clutter is the completely polarized wave, the performance of clutter suppression for PST-JDP method is insensitive to the input CNR for Figure 8. However, when the clutter is the partially polarized wave and the normalized target Doppler frequency is small, both performance of optimal PST-JDP and optimum space-time processing are sensitive to the input CNR.

(iv) The radar system for PST-JDP increases the DOF to suppress clutter. The DOF of system is twice to the number of elements. When clutter is high degree of polarization or completely polarized wave, the DOF of clutter for PST-JDP system is approximately equal to the DOF of space time processing system. Therefore, the performance for PST-JDP is superior to optimum space-time processing.

ACKNOWLEDGMENT

This work was partly supported by the National Natural Science Foundation of China under Grants 60736006 and 60901072. The authors are deeply in debit to Dr. Y. Wu in Beijing Research Institute at Huawei Technologies for his helpful comments and suggestions.

REFERENCES

1. Liu, Z., X. Wei, and X. Li, "Adaptive clutter suppression for airborne random pulse repetition interval radar based on compressed sensing," *Progress In Electromagnetics Research*, Vol. 128, 291–311, 2012.
2. Morin, X., E. Pottier, J. Saillard, C. Pasdeloup, and C. Delhote, "Polarimetric detection of slowly moving targets embedded in stationary ground clutter," *Progress In Electromagnetics Research*, Vol. 16, 1–33, 1997.
3. Yang, R. Y., H. Kuan, C. Y. Hung, and C. S. Ye, "Design of dualband bandpass filters using a dual feeding structure and embedded uniform impedance resonators," *Progress In Electromagnetic Research*, Vol. 105, 93–102, 2010.
4. Gong, Q. Y. and Z. D. Zhu, "Study STAP algorithm on interference target detect under nonhomogenous environment," *Progress In Electromagnetics Research*, Vol. 99, 211–224, 2009.
5. Giuli, D., "Polarization diversity in radars," *IEEE Proceeding*, Vol. 74, No. 2, 246–249, 1986.
6. Gherardelii, M., D. Giuli, and M. Fossi, "Suboptimum adaptive polarisation cancellers for dual-polarisation radars," *IEE Proceeding*, Vol. 135, No. 1, 60–72, 1988.
7. Poelman, A. J., "Virtual polarisation adaptation a method of increasing the detection capability of a radar system through polarisation-vector processing," *IEE Proc. Commun., Radar & Signal Process.*, Vol. 128, No. 5, 261–270, 1981.
8. Poelman, A. J., "Polarisation-vector translation in radar systems," *IEE Proceeding*, Vol. 130, No. 2, 161–166, 1983.
9. Poelman, A. J. and J. R. F. Guy, "Multinotch logic-product polarization suppression filters: A typical design example and its performance in a rain clutter environment," *IEE Proceeding*, Vol. 131, No. 4, 383–396, 1984.
10. Maio, A. D. and G. Ricci, "A polarimetric adaptive matched filter," *Signal Processing*, Vol. 81, No. 12, 2583–2589, 2001.
11. Wang, X. S., Y. L. Chang, D. H. Dai, et al., "Band characteristics

of SINR polarization filter," *IEEE Transactions on Antennas and Propagation*, Vol. 55, No. 4, 1148–1154, 2007.

12. Secmen, M. and A. Hizal, "A dual-polarized wide-band patch antenna for indoor mobile communication applications," *Progress In Electromagnetics Research*, Vol. 100, 189–200, 2010.
13. Moradi, K. and S. Nikmehr, "A dual-band dual-polarized microstrip array antenna for base stations," *Progress In Electromagnetic Research*, Vol. 123, 527–541, 2012.
14. Chi, L. P., S. S. Bor, S. M. Deng, C.-L. Tsai, P.-H. Juan, and K.-W. Liu, "A wideband wide-strip dipole antenna for circularly polarized wave operations," *Progress In Electromagnetics Research*, Vol. 100, 69–82, 2010.
15. Novak, L. M., M. C. Burl, and W. W. Irving, "Optimal polarimetric processing for enhanced target detection," *IEEE Transactions on Aerospace and Electronic Systems*, Vol. 29, No. 1, 234–244, 1993.
16. Hurtado, M. and A. Nehorai, "Polarimetric detection of targets in heavy inhomogeneous clutter," *IEEE Transactions on Signal Processing*, Vol. 56, No. 4, 1349–1361, 2008.
17. Xiao, J. J. and A. Nehorai, "Joint transmitter and receiver polarization optimization for scattering estimation in clutter," *IEEE Transactions on Signal Processing*, Vol. 57, No. 10, 4142–4147, 2009.
18. Wang, J. and A. Nehorai, "Adaptive polarimetry design for a target in compound-Gaussian clutter," *Signal Processing*, Vol. 89, No. 6, 1061–1069, 2009.
19. Alvarez-Perez, J. L., "Coherence, polarization and statistical independence in Cloude-Pottier's radar polarimetry," *IEEE Transactions on Geoscience and Remote Sensing*, Vol. 49, No. 1, 426–441, 2011.
20. Klemm, R., "Principles of space-time adaptive processing," *IEE Radar, Sonar, Navigation and Avionics 12*, IEE Press, London, 2002.
21. Xu, Z. H. and X. S. Wang, et al., "Filtering performance of polarization sensitive array: Completely polarized case," *Acta Electronic Sinica*, Vol. 32, No. 8, 1130–1134, 2004.
22. Zhang, X., Y. Shi, and D. Xu, "Novel blind joint direction of arrival and polarization estimation for polarization-sensitive uniform circular array," *Progress In Electromagnetics Research*, Vol. 86, 19–37, 2008.
23. Peng, H. L., W. Y. Yin, J. F. Mao, D. Huo, X. Hang, and

L. Zhou, "A compact dual-polarized broadband antenna with hybrid beam-forming capabilites," *Progress In Electromagnetics Research*, Vol. 118, 253–271, 2011.

24. Gu, Y.-J., Z.-G. Shi, K. S. Chen, and Y. Li, "Robust adaptive beamforming for steering vector uncertainties based on equivalent DOAs method," *Progress In Electromagnetics Research*, Vol. 79, 277–290, 2008.
25. Lizzi, L., F. Viani, M. Benedetti, P. Rocca, and A. Massa, "The M-DSO-ESPRIT method for maximum likelihood DOA estimation," *Progress In Electromagnetics Research*, Vol. 80, 477–497, 2008.
26. Pastina, D., P. Lombardo, and T. Bucciarelli, "Adaptive polarimetric target detection with coherent radar. I: Detection against Gaussian background," *IEEE Transactions on Aerospace and Electronic Systems*, Vol. 37, No. 4, 1194–1206, 2001.
27. Lombardo, P., D. Pastina, and T. Bucciarelli, "Adaptive polarimetric target detection with coherent radar. II: Detection against non-Gaussian background," *IEEE Transactions on Aerospace and Electronic Systems*, Vol. 37, No. 4, 1207–1220, 2001.
28. Brennan, L. E. and I. S. Reed, "Theory of adaptive radar," *IEEE Transactions on Aerospace and Electronic Systems*, Vol. 9, No. 2, 237–252, 1973.
29. Reed, I. S., J. D. Mallett, and L. E. Brennan, "Rapid convergence rate in adaptive arrays," *IEEE Transactions on Aerospace and Electronic Systems*, Vol. 10, No. 6, 853–863, 1974.
30. Kelly, E. J., "An adaptive detection algorithm," *IEEE Transactions on Aerospace and Electronic Systems*, Vol. 22, No. 1, 115–127, 1986.
31. Klemm, R., "Adaptive airborne MTI: An auxiliary channel approach," *IEE Processing*, Vol. 134, No. 3, 269–276, 1987.
32. Ward, J., "Space-time adaptive processing for airborne radar," Lincoln Laboratory, Technical Report 1015, 1994.
33. Wu, J. X., T. Wang, and Z. Bao, "FFT implementation of Doppler dependent pre-Doppler STAP," *Signal Processing*, Vol. 92, No. 1, 281–287, 2012.
34. Fa, R., R. C. de Lamare, and L. Wang, "Reduced-rank STAP schemes for airborne radar based on switched joint interpolation, decimation and filtering algorithm," *IEEE Transactions on Signal Processing*, Vol. 58, No. 8, 4182–4194, 2010.
35. Beau, S. and S. Marcos, "Range dependent clutter rejection using range-recursive space-time adaptive processing (STAP)

algorithms," *Signal Processing*, Vol. 90, No. 1, 57–68, 2010.

36. Sun, K., H. D. Meng, Y. L. Wang, et al., "Direct data domain STAP using sparse representation of clutter spectrum," *Signal Processing*, Vol. 91, No. 9, 2222–2236, 2011
37. Sun, K., H. D. Meng, F. D. Lapierre, et al., "Registration-based compensation using sparse representation in conformal-array STAP," *Signal Processing*, Vol. 91, No. 10, 2268–2276, 2011.
38. Stoica, P., J. Li, X. M. Zhu, and J. R. Guerci, "On using a priori knowledge in space-time adaptive processing," *IEEE Transactions on Signal Processing*, Vol. 56, No. 6, 2598–2602, 2008.
39. Bidon, S., O. Besson, and J. Y. Tourneret, "Knowledge-aided STAP in heterogeneous clutter using a hierarchical Bayesian algorithm," *IEEE Transactions on Aerospace and Electronic Systems*, Vol. 47, No. 3, 1863–1879, 2011.
40. Wu, Y., J. Tang, and Y. N. Peng, "On the essence of knowledge-aided clutter covariance estimate and its convergence," *IEEE Transactions on Aerospace and Electronic Systems*, Vol. 47, No. 1, 569–585, 2011.
41. Park, H. R. and H. Wang, "Adaptive polarisation-space-time domain radar target detection in inhomogeneous clutter environments," *IEE Proceedings Radar, Sonar and Navigation*, Vol. 153, No. 1, 35–43, 2006.
42. Park, H. R., J. Li, and H. Wang "Polarization-space-time domain generalized likelihood ratio detection of radar target," *Signal Processing*, Vol. 41, No. 2, 153–164, 1995.
43. Park, H. R., H. Wang, and J. Li, "An adaptive polarization-space-time processor for radar system," *Antennas and Propagation Society International Symposium*, No. 2, 698–701, 1993.
44. Kuebel, D., "Properties of the degree of cross-polarization in the spacetime domain," *Optics Communications*, 3397–3401, 2009.
45. Slepian, D. and H. O. Pollak, "Prolate spheroidal wave functions, Fourier analysis and uncertainty — I," *Bell Svst. Tech. J.*, Vol. 40, No. 1, 43–63, 1961.
46. Slepian, D., "Prolate spheroidal wave functions, Fourier analysis and uncertainty — V," *Bell Svst. Tech. J.*, Vol. 57, No. 5, 1371–1429, 1978.
47. Fancourt, C. L. and J. C. Principe, "On the relationship between the Karhunen-Loeve transform and the prolate spheroidal wave function," *Proceedings of IEEE International Conference on Acoustics, Speech, and Signal Processing (ICASSP)*, 261–264, 2000.